crystals

MDPI

Article

Mode-Locked YDFL Using Topological Insulator Bismuth Selenide Nanosheets as the Saturable Absorber

Hazlihan Haris [1], Malathy Batumalay [2], Sin Jin Tan [3], Arni Munira Markom [4], Ahmad Razif Muhammad [5], Sulaiman Wadi Harun [6], Megat Muhammad Ikhsan Megat Hasnan [1] and Ismail Saad [1,*]

[1] Faculty of Engineering, Universiti Malaysia Sabah (UMS), Kota Kinabalu 88400, Sabah, Malaysia; hazlihanharis@ums.edu.my (H.H.); megatikhsan@ums.edu.my (M.M.I.M.H.)
[2] Faculty of Data Science and IT, INTI International University, Nilai 71800, Selangor, Malaysia; malathy.batumalay@newinti.edu.my
[3] School of Engineering, UOW Malaysia KDU University College, Shah Alam 40150, Selangor, Malaysia; sj.tan@kdu.edu.my
[4] School of Electrical Engineering, College of Engineering, Kampus Pasir Gudang, Universiti Teknologi MARA, Masai 81750, Johor, Malaysia; arnimunira@uitm.edu.my
[5] Institute of Microengineering and Nanoelectronics (IMEN), Universiti Kebangsaan Malaysia (UKM), Bangi 43600, Selangor, Malaysia; a.razif@ukm.edu.my
[6] Department of Electrical Engineering, University of Malaya, Kuala Lumpur 50603, Selangor, Malaysia; swharun@um.edu.my
* Correspondence: ismail_s@ums.edu.my

Abstract: Fiber lasers have long remained relevant for various applications worldwide in many industries. This paper presents a mode-locked ytterbium-doped fiber laser (YDFL) using our home-made topological insulator Bi_2Se_3 nanosheets (TI Bi_2Se_3) as the saturable absorber. The fabricated TI Bi_2Se_3 is transported to the end of the fiber ferrule using an optical deposition process, which is a key ingredient for initiating a pulsed fiber laser. With a pump power of 211.1 mW, the captured repetition rate and pulse width are 8.3 MHz and 6.2 ns, respectively. The length of the setup configuration is approximately 20 m, which corresponds to an output power measurement of 12.4 mW with a calculated pulse energy of 1.5 nJ. There are no significant Kelly sidebands, but the strong stability of the pulsed laser is defined by a high signal-to-noise ratio (SNR) of around 60.35 dB.

Keywords: mode-locked fiber laser; saturable absorber; topological insulator

Citation: Haris, H.; Batumalay, M.; Tan, S.J.; Markom, A.M.; Muhammad, A.R.; Harun, S.W.; Megat Hasnan, M.M.I.; Saad, I. Mode-Locked YDFL Using Topological Insulator Bismuth Selenide Nanosheets as the Saturable Absorber. *Crystals* **2022**, *12*, 489. https://doi.org/10.3390/cryst12040489

Academic Editor: Chunhui Yang

Received: 4 March 2022
Accepted: 30 March 2022
Published: 1 April 2022

1. Introduction

Pulsed-fiber laser technology has evolved dramatically over the years due to its efficiency, accuracy, reliability, and compatibility with many applications across many industries. Q-switched or mode-locked are both types of these remarkable fiber lasers, with individual interest depending on the pulses' repetition rates and pulse widths. Q-switched pulsed-fiber lasers typically have a kilohertz repetition rate and a nanoseconds pulse width, which is somewhat slow and large compared to mode-locked pulses. Still, they have their advantages, such as large power output and pulsed energy, suitable for use in dentistry for pain relief, environmental monitoring, and medical diagnostics [1,2]. Mode-locked pulsed lasers are now used extensively in various applications, including communications, medical treatment, medical surgery, and industrial micromachining. Mode-locked pulses have a high repetition rate in the megahertz range and narrow pulse width in the picosecond range.

Nonlinear polarization rotation (NPR) and saturable absorber (SA) are two common methods for generating mode-locked pulses [3,4]. However, the SA method attracts more attention due to its simple experimental configuration and high probability of generating the fiber laser pulses. For more than three decades, these pulses have been demonstrated with

carbon-based materials such as graphene [5–7], carbon nanotubes (CNTs) [8,9], and silicon–germanium (SiGe) [10]. Aside from being used as the SA, they are also used to enhance the operation of field effect transistors (FETs) [11]. The discovery of graphene led to the development of other novel 2D materials, such as topological insulators (TIs) [12,13], transition metal dichalcogenides (TMDs) [14–17], black phosphorus (BP) [18,19], MXenes [20,21], and Max phase [22,23]. These two-dimensional materials possess exceptional electrical and optical properties that make them suitable for use as sensors [24], modulators [25], photodiodes [26], and transistors [27]. For example, graphene is applied to a tapered fiber to enable temperature measurement [28], and MXene is used for an all-optical wavelength converter, useful for future development of the direct optical signal-processing applications [29]. The different sample thicknesses of rare earth oxide also have been investigated as a potential saturable absorber candidate for output laser performance [30]. The latest work by Zhang et al. also shows the success of implementing the organic porous crystal structure class materials (NiO–MOF) as high-performance ultrafast lasers, achieving the harmonic mode-locking at femtoseconds level [31].

TI is an intriguing two-dimensional material with a solo Dirac cone and a big band-gap comparable to graphene. Furthermore, TI is a material that has a bulk band gap like an insulator but conducts at its surface, making it a promising candidate for basic research and applied physics. For instance, Bi_2Se_3 with ΔE~0.3 eV exhibits low saturation intensity, high modulation depth, and broadband saturable absorption properties. TI has proven to be an effective and efficient SA for initiating Q-switching and mode-locking [32,33]. The pervasive way to integrate SA into a fiber laser cavity is to place a thin film of SA between two fiber connectors. Other integration methods are used to coat 2D materials on tapered and D-shaped fibers [34]. In this work, a TI Bi_2Se_3 was deposited onto the fiber ferrule and integrated into ytterbium-doped fiber (YDF) to create a laser pulse. Mode-locking is observed at a repetition rate of 8.3 MHz and a pulse width in the picosecond range.

2. Preparation of TI Bi_2Se_3

The Bi_2Se_3 nanosheets (Sigma-Aldrich, Subang Jaya, Malaysia) were used as our saturable absorber optical component. First, 7 mg of Bi_2Se_3 nanosheets were mixed with 60 mL of isopropyl alcohol using the hot plate stirrer. This blend was stirred continuously for one day using a magnetic stirrer and further subjected to ultrasonic treatment for six hours, resulting in a Bi_2Se_3 suspension. Subsequently, this Bi_2Se_3 suspension was placed in an ultrasonic bath with a frequency of 40 kHz for about 30 min to yield a heterogenous Bi_2Se_3 mixture.

The optical deposition process was performed by injecting 60 mW of 980 nm laser at one end of the SMF-28 fiber ferrule and immersing another end onto the TI suspension for 30 min. The fiber ferrule was then removed from the TI suspension and allowed to evaporate for another 20 min. This procedure was repeated three times to improve the Bi_2Se_3 adhesion to the fiber core.

Next, the following process was carried out to simplify our SA's characterization. The Bi_2Se_3 thin film was formed using the spin coater machine to produce the homogenous distribution of Bi_2Se_3, assisted with polyvinyl alcohol film, and later placed in an oven for further drying. Field emission scanning electron microscopy (FESEM), Raman spectroscopy, and energy-dispersive x-ray (EDX) analysis were used to characterize the SA. Figure 1 shows the results of the characterization. The FESEM image of Bi_2Se_3 synthesized from Bi_2Se_3 nanosheets revealed layers similar to the complex flakes shown in Figure 1a. The compositions of Bi_2Se_3 were analyzed by EDX and are shown in Figure 1b. According to the atomic force microscopy (AFM) topography measurement in Figure 1c, a few-layer of Bi_2Se_3 was found to have a thickness of about 3.8 nm. The Raman spectroscopy of Bi_2Se_3 in Figure 1d shows that multiple vibration modes have been assigned in three apparent peaks as indicated in Raman's rule choices [35]: A_{1g}^1 mode at 72 cm^{-1}, E_g^2 mode at 132 cm^{-1}, and A_{1g}^2 mode at 173 cm^{-1}. The frequency range scanned was examined in three prominent peaks and was consistent with previously published work [36].

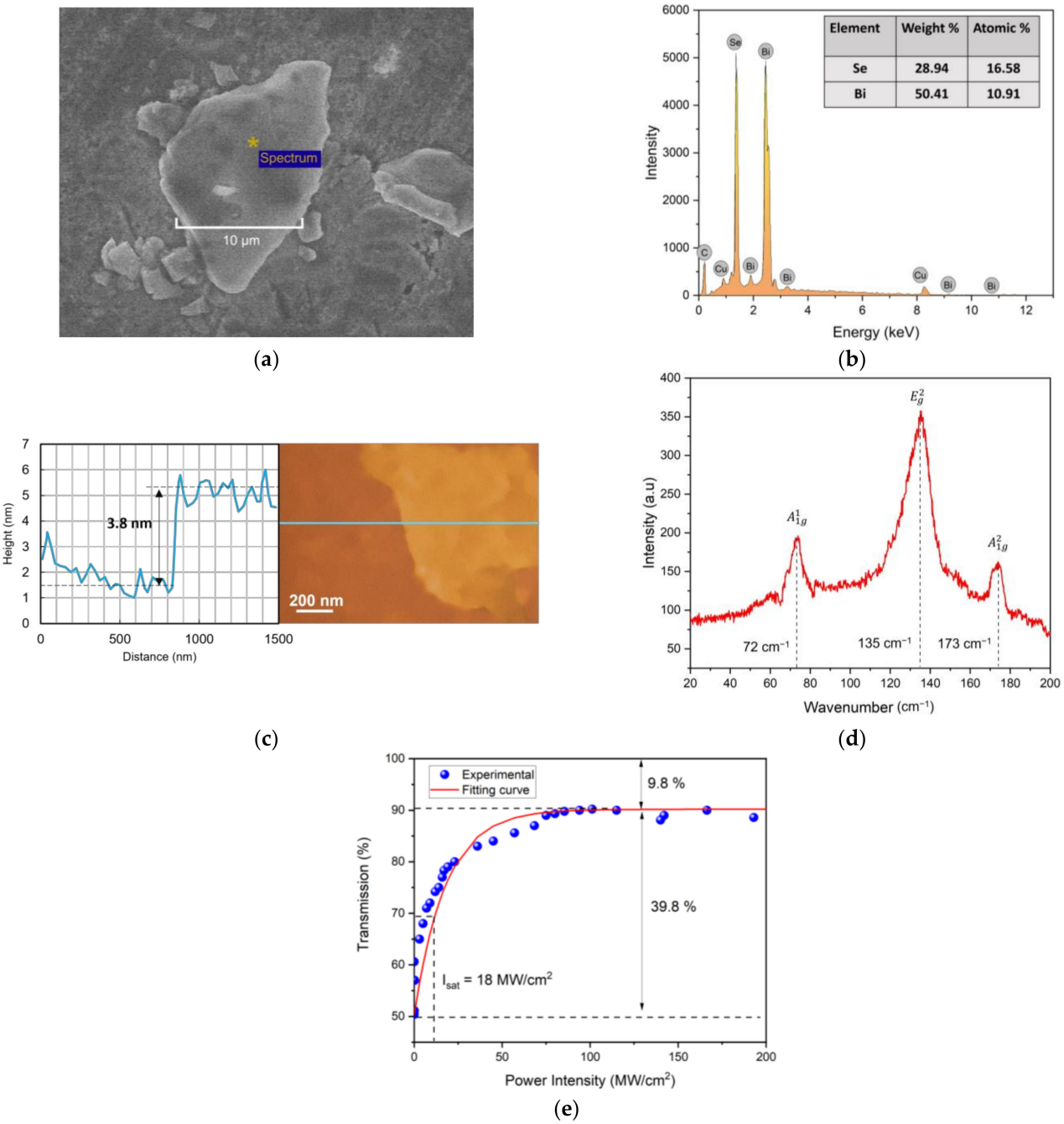

Figure 1. Characterization of layered TI-Bi_2Se_3 (**a**) FESEM image shows flakes of Bi_2Se_3 at 10 µm scale and mapping spectrum for EDX measurement denoted with asterisk; (**b**) EDX spectrum; (**c**) AFM topography with an interface between PVA and Bi_2Se_3; (**d**) Raman spectrum; (**e**) nonlinear response profile.

The nonlinear optical response property for Bi_2Se_3 was investigated using the twin balance detection method [37]. Figure 1e shows the obtained nonlinear transmission curve. The curve is fitted with the following equation $T(I) = 1 - (\alpha_s \times \exp(-I/I_{sat}) - \alpha_{ns})$. Where T(I) is the transmission, α_s is the modulation depth, I is the input intensity, I_{sat} is the saturation intensity, and α_{ns} is the non-saturable absorption. Upon fitting the measured experimental data to the above equation, it can be concluded that the I_{sat}, α_s, and α_{ns} for Bi_2Se_3 are 18 MW/cm^2, 39.8%, and 9.8%, respectively.

3. Experimental Setup

Figure 2 illustrates the experimental configuration of the proposed TI-based SA mode-locked YDFL. The gain medium used was 3-m-long YDF. The remaining optical fiber components consisted of a wavelength division multiplexer (WDM), a polarization controller (PC), an isolator, and a 95:5 coupler. A 980-nm laser diode (LD) was injected into the YDF via the 980/1064-nm WDM. At 1020 nm, the absorption of ytterbium ions was 23 dB/m, while the core and cladding diameters of the YDF used were 4 µm and 125 µm. A deposited TI Bi_2Se_3 SA is positioned between the additional SMF and PC. An additional 15-m-long SMF-28 was introduced to balance the cavity's dispersion and nonlinearity, leading to stable mode-locking pulses in the current cavity.

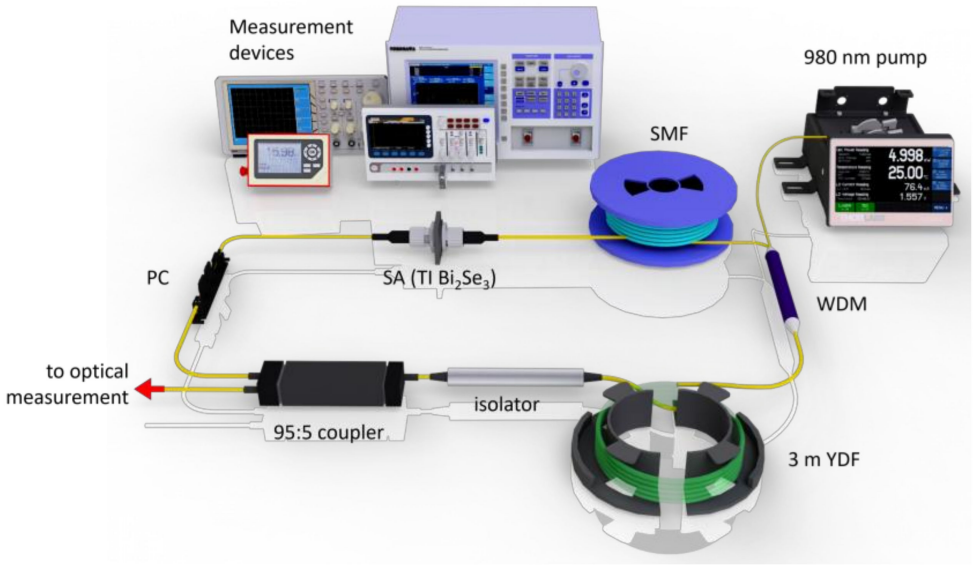

Figure 2. Experimental configuration for mode-locked YDFL.

The role of the isolator was to restrict the direction of light propagation, while the polarization of the light was controlled by PC. We extracted 5% of the light out from the configuration via the 95:5 coupler for monitoring and characterization. The other 95% of the light was circulated back into the laser cavity. An optical spectrum analyzer (OSA-Yokogawa AQ6370B, Tokyo, Japan, 0.02 nm resolution) was used to characterize the pulse spectrum. A photodetector 1.2 GHz bandwidth (Thorlabs DET01CFC, Bergkirchen, Germany) with a standard oscilloscope (Tektronix TDS3052C, Boston, MA, USA) was used to examine the pulse train measurement in an electrical signal form plugged into a 50:50 output coupler. Pulse stability was determined using a radio frequency (RF) spectrum analyzer. The cavity consisted of 20-m length of all-fiber components and operated in anomalous dispersion with group delay dispersion (GDD) of -0.3042 ps^2.

4. Results and Discussion

To examine the pulse threshold, the pump power was increased steadily. When the pump power reached 110.5 mW, the self-started mode-locking operation was observed as continuous-wave (CW) lasing broadened in the OSA. The mode-locked operation was still steadily maintained while the pump was progressively increased until a maximum level of 211 mW was reached. Figure 3 shows the mode-locked optical spectrum captured at 211 mW. The central operating wavelength of the pulse spectrum was found to be 1051.7 nm with a 3 dB bandwidth measurement of 1.04 nm. No significant Kelly sidebands were observed in the optical spectrum. Figure 4 shows the pulse train profile at a pump power of 211 mW. The full resolution of the pulse train is shown in Figure 4a, whereas the close-up train is shown in Figure 4b. The peak-to-peak spacing on the oscilloscope trace was measured at 120.5 ns, corresponding to a pulse repetition rate of 8.3 MHz.

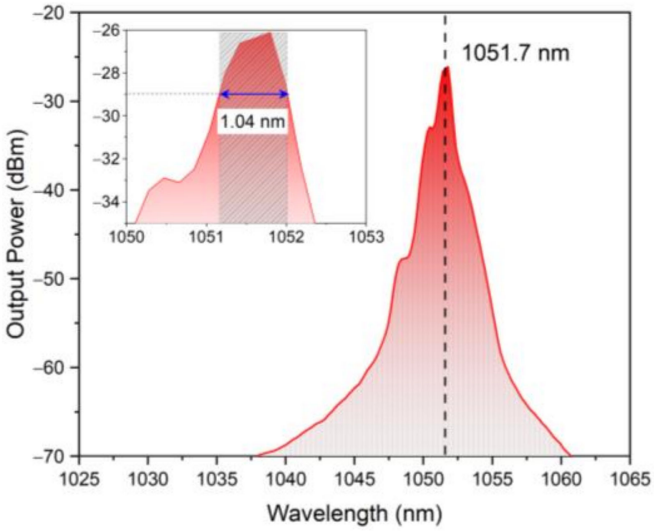

Figure 3. The optical spectrum of mode-locked YDFL with a central wavelength of 1051.7 nm. The inset shows the 3-dB bandwidth measurement.

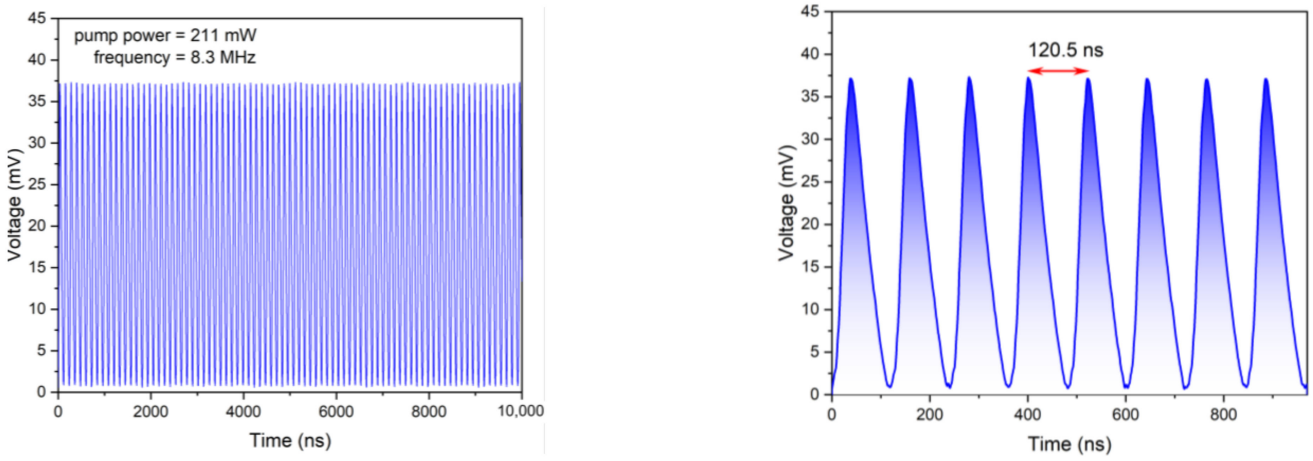

(**a**) (**b**)

Figure 4. A pulse train of mode-locked YDFL: (**a**) full resolution, (**b**) close-up pulse train at 900-ns span.

This repetition rate was consistent with the overall configuration length and showed that the mode-locked YDFL was operating at the fundamental repetition rate. At 211 mW pump power, mode-locked operation remained stable. The magnified view of the oscillation trace showed that the pulse width was 6.2 ns. The pulse width measurement on the oscilloscope was wider compared to the real pulse width value due to the optical measurement devices' limitations. The minimum estimated pulse width was predicted using a theoretical calculation of time–bandwidth product (TBP), assuming that the pulse shape is the sech^2 pulse profile. The analysis showed that the pulse width from the laser configuration should be approximately 1.11 ps.

The stability of the pulse was verified with an RF spectrum analyzer as shown in Figure 5. The pulse's fundamental frequency at 8.3 MHz, with a signal-to-noise ratio (SNR) of about 60.35 dB was recorded. It is worth noting that the laser operation was switched to CW when SA was removed from the configuration. This verified that the fabricated SA was responsible for the mode-locking operation, and it cannot be initiated without the presence of SA.

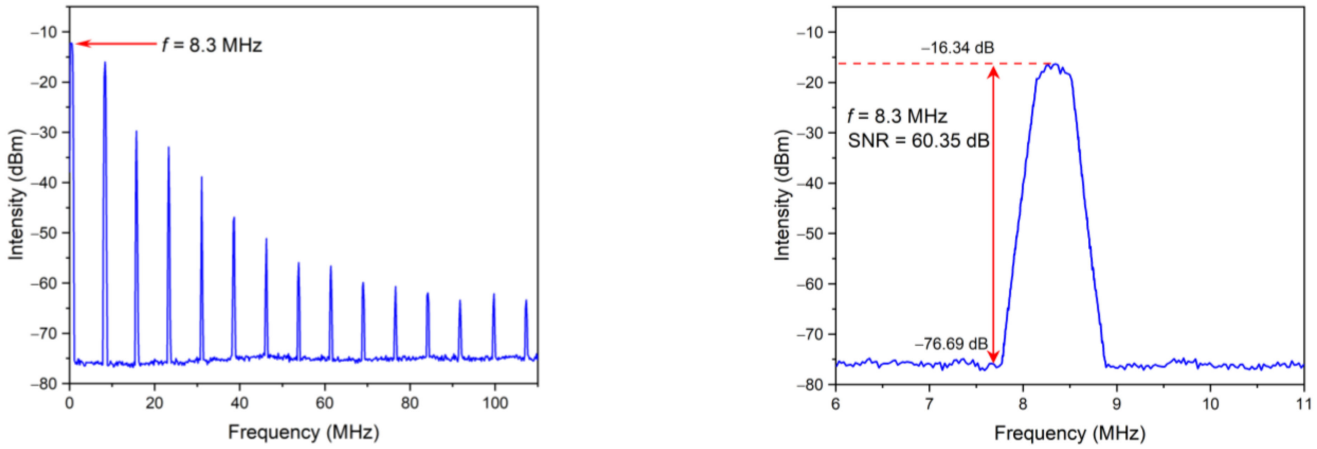

(**a**) (**b**)

Figure 5. RF spectrum for SNR measurement (**a**) 110 MHz spectrum resolution; (**b**) single spectrum at fundamental frequency of 8.3 MHz.

Figure 6 represents the relationship between average laser output power and pulse energy as a function of pump powers. Both the output power and the pulse energy increase linearly with increasing pump power. At maximum available pump power of 211 mW, recorded output power is 12.4 mW, corresponding to the 1.5-nJ calculated pulse energy.

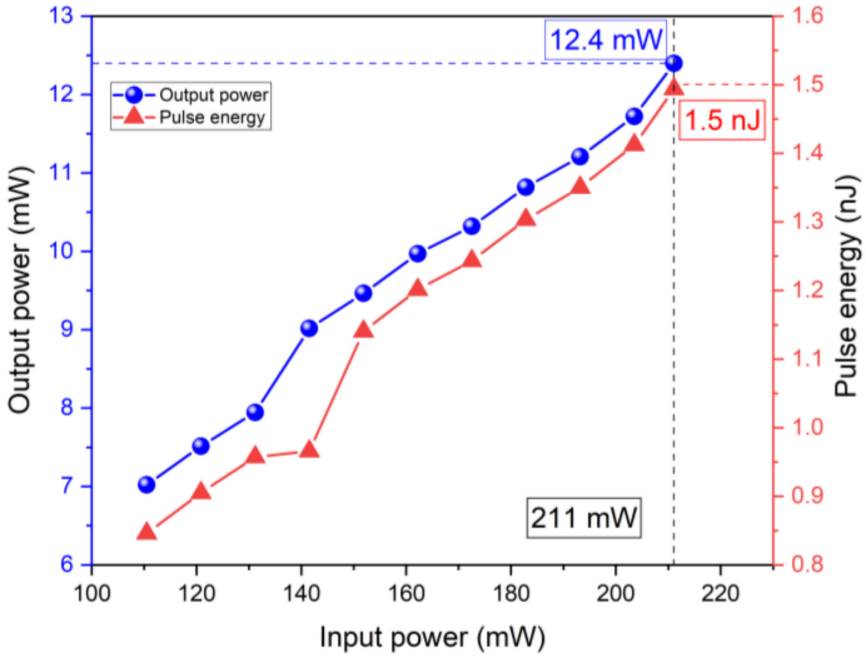

Figure 6. Average power and pulse energy of mode-locked YDFL.

Table 1 below shows the compilation of work reported on mode-locked YDFL at the 1 µm region using various SAs. SAs have proven their capability to induce ultrafast mode-locking at 1 µm, specifically graphene and TI, where they exhibit broadband saturable absorption properties. Both graphene and TI SA demonstrated the ability to generate ultrafast mode-locking at 1 µm. The threshold mode-locking in our work was relatively low at 110.5 mW compared to other TI-based SA.

Table 1. Ultrafast mode-locked laser performances at 1 μm using various SAs.

SA Material	Integration Method	Operating Wavelength	3 dB Bandwidth	Threshold (mW)	Pulse Width	Repetition Rate	Ref.
Graphene	Thin film	1964.9 nm	0.19 nm	567 mW	0.9–6.8 ns	927 kHz	[38]
GO	Thin film	1064.1 nm	0.477 nm	137 mW	2.3 ns	1.072 MHz	[39]
Graphene	Thin film	1069.5 nm	1.29 nm	45 mW	580 ps	0.9 MHz	[40]
Graphene	Tapered fiber	1061.8 nm, 1068.8 nm	4.5 nm, 2.16 nm	263 mW	2.64 ns	1.78 MHz	[41]
GO	Thin film	1077.68 nm	1.22 nm	106.5 mW	2.0 ns	1.583 MHz	[42]
GO	Thin film	1059.7 nm	1.93 nm	45 mW	189 ps	10.05 MHz	[43]
TMD MoS_2	Thin film	1029.3 nm	2.3 nm	55 mW	336.5 ps	2.025 MHz	[44]
TMD PDS_2	Side-polished fiber	1033 nm	3.7 nm	160 mW	375 ps	24.4 MHz	[45]
TMD $PdSe_2$	Thin film	1067.37 nm	5.22 nm	135 mW	767.7 ps	3.77 MHz	[46]
BP	Thin film	1085.58 nm	0.23 nm	1322 mW	26 ns	13.5 MHz	[47]
BP	Thin film	1030.6 nm	0.11 nm	200 mW	400 ps	46.3 MHz	[47]
BP	Thin film	1067.1 nm	0.11 nm	258.6 mW	77.2 ns	0.39 MHz	[48]
TI $Bi2Se_3$	Thin film	1031.7 nm	2.5 nm	153 mW	46 ps	44.6 MHz	[49]
TI $Bi2Te_3$	SPF	1057.82 nm	3.69 nm	200 mW	230 ps	1.44 Mhz	[50]
Ti $Bi2Te_3$	Tapered fiber	1052.5 nm	1.245 nm	230 mW	317 ps	19.8 MHz	[51]
Ti $Sb2Te_3$	SPF	1039.4 nm	4.25 nm	320 mW	380 ps	17.07 MHz	[52]
Ti $Bi2Te_3$	Tapered fiber	1063.4 nm	2.24 nm	220 mW	5.47 ns	6.2 MHz	[53]
TI $Bi2Se_3$	Thin film	1065.08 nm	0.025 nm	105 mW	398 ns	527 kHz	[54]
TI Bi_2Se_3	Optical deposition	1051.7	1.04 nm	110.5 mW	6.2 ns	8.3 MHz	This work

5. Conclusions

A homemade fabricated TI Bi_2Se_3 SA succeeded in initiating a mode-locked YDFL. The constructed mode-locked YDFL lased stably in a laboratory environment with a basic repetition rate of 8.3 MHz and a pulse width of 6.2 ns. The maximum output power and pulse energy are 12.4 mW and 1.5 nJ, with a pump power of 211 mW, respectively. In addition, the SNR from the RF spectrum is 60.35 dB, which indicates the strong stability of the mode-locking pulse to the experimental configuration.

Author Contributions: Conceptualization, methodology and validation, H.H. and S.J.T.; resources, I.S.; formal analysis, M.M.I.M.H.; writing—original draft preparation, H.H.; writing—review and editing, A.M.M.; visualization, A.R.M.; supervision, S.W.H.; project administration and funding acquisition, I.S. and M.B. All authors have read and agreed to the published version of the manuscript.

Funding: This research was funded by Niche Research Fund Scheme, Universiti Malaysia Sabah (UMS), grant number SDN00286 and Postgraduate Research Grant Scheme (UMSGreat), grant number GUG0444-1/2020. The APC was funded by Ismail Saad.

Data Availability Statement: Not applicable.

Acknowledgments: The authors would also like to thank the research facility from Photonics Engineering Laboratory, University of Malaya (UM), Nanophotonics Laboratory, Institute of Microengineering and Nanoelectronics, Universiti Kebangsaan Malaysia (UKM), and INTI International University for the research support.

Conflicts of Interest: The authors declare no conflict of interest.

References

1. Mirjanic, V.; Sreckovic, M.; Mirjanic, D.; Bugarinovic, A.; Druzijanic, D.; Mitic, V.V. Chosen applications and approaches to modeling lasers in dentistry. *Mod. Phys. Lett. B* **2021**, *35*, 2150329. [CrossRef]
2. Zhang, Y.P.; Liu, Y.F.; Jia, D.G.; Yu, T.Y.; Huang, Y.D.; Zhang, Z.Y.; Wang, R.X. Electrically controlled tunable optical parametric oscillator (3.0–6.7 μm) based on BaGa4Se7 crystal pumped by a Q-switch Nd: YAG laser. In *AOPC 2020: Advanced Laser Technology and Application*; SPIE: Bellingham, WA, USA, 2020; Volume 11562.
3. Tan, S.J.; Harun, S.W.; Arof, H.; Ahmad, H. Switchable Q-switched and mode-locked erbium-doped fiber laser operating in the L-band region. *Chin. Opt. Lett.* **2013**, *11*, 073201.
4. Tan, S.J.; Tiu, Z.C.; Harun, S.W.; Ahmad, H. Sideband-controllable soliton pulse with bismuth-based erbium-doped fiber. *Chin. Opt. Lett.* **2015**, *13*, 111406. [CrossRef]

5. Adnan, N.; Bidin, N.; Taib, N.; Haris, H.; Fakaruddin, M.; Hashim, A.; Krishnan, G.; Harun, S. Passively Q-switched flashlamp pumped Nd: YAG laser using liquid graphene oxide as saturable absorber. *Opt. Laser Technol.* **2016**, *80*, 28–32. [CrossRef]
6. Taib, N.A.M.; Bidin, N.; Haris, H.; Adnan, N.N.; Ahmad, M.F.S.; Harun, S.W. Multi-walled carbon nanotubes saturable absorber in Q-switching flashlamp pumped Nd: YAG laser. *Opt. Laser Technol.* **2016**, *79*, 193–197. [CrossRef]
7. Markom, A.M.; Latiff, A.A.; Muhammad, A.R.; Ahmad, M.T.; Yusoff, Z.M.; Paul, M.C.; Dhar, A.; Das, S.; Harun, S.W. Q-switched Zirconia-Yttria-Aluminium-Erbium-doped pulsed fiber laser with a pencil-core of graphene as saturable absorber. *Optoelectron. Adv. Mater.-Rapid Commun.* **2020**, *14*, 1–5.
8. Dai, L.L.; Huang, Z.N.; Huang, Q.Q.; Zhao, C.; Rozhin, A.; Sergeyev, S.; Al Araimi, M.; Mou, C.B. Carbon nanotube mode-locked fiber lasers: Recent progress and perspectives. *Nanophotonics* **2021**, *10*, 749–775. [CrossRef]
9. Haris, H.; Anyi, C.; Ali, N.; Arof, H.; Ahmad, F.; Nor, R.; Zulkepely, N.; Harun, S. Passively Q-switched erbium-doped fiber laser at L-band region by employing multi-walled carbon nanotubes as saturable absorber. *Optoelectron. Adv. Mater.-Rapid Commun.* **2014**, *8*, 1025–1028.
10. Guo, Y.X.; Li, X.H.; Guo, P.L.; Zheng, H.R. Supercontinuum generation in an Er-doped figure-eight passively mode-locked fiber laser. *Opt Express* **2018**, *26*, 9893–9900. [CrossRef]
11. Deng, T.; Zhang, Z.H.; Liu, Y.X.; Wang, Y.X.; Su, F.; Li, S.S.; Zhang, Y.; Li, H.; Chen, H.J.; Zhao, Z.R.; et al. Three-Dimensional Graphene Field-Effect Transistors as High-Performance Photodetectors. *Nano Lett.* **2019**, *19*, 1494–1503. [CrossRef]
12. Haris, H.; Arof, H.; Muhammad, A.R.; Anyi, C.L.; Tan, S.J.; Kasim, N.; Harun, S.W. Passively Q-switched and mode-locked Erbium-doped fiber laser with topological insulator Bismuth Selenide (Bi2Se3) as saturable absorber at C-band region. *Opt. Fiber Technol.* **2019**, *48*, 117–122. [CrossRef]
13. Jin, L.; Ma, X.; Zhang, H.; Zhang, H.; Chen, H.; Xu, Y. 3 GHz passively harmonic mode-locked Er-doped fiber laser by evanescent field-based nano-sheets topological insulator. *Opt. Express* **2018**, *26*, 31244–31252. [CrossRef] [PubMed]
14. Liu, W.; Pang, L.; Han, H.; Bi, K.; Lei, M.; Wei, Z. Tungsten disulphide for ultrashort pulse generation in all-fiber lasers. *Nanoscale* **2017**, *9*, 5806–5811. [CrossRef] [PubMed]
15. Liu, W.; Liu, M.; OuYang, Y.; Hou, H.; Ma, G.; Lei, M.; Wei, Z. Tungsten diselenide for mode-locked erbium-doped fiber lasers with short pulse duration. *Nanotechnology* **2018**, *29*, 174002. [CrossRef] [PubMed]
16. Liu, M.; Wu, H.; Liu, X.; Wang, Y.; Lei, M.; Liu, W.; Guo, W.; Wei, Z. Optical properties and applications of SnS_2 SAs with different thickness. *Opto-Electron. Adv.* **2021**, *4*, 200029-1. [CrossRef]
17. Li, L.; Pang, L.; Wang, R.; Zhang, X.; Hui, Z.; Han, D.; Zhao, F.; Liu, W. Ternary Transition Metal Dichalcogenides for High Power Vector Dissipative Soliton Ultrafast Fiber Laser. *Laser Photonics Rev.* **2021**, *16*, 2100255. [CrossRef]
18. Hisyam, M.B.; Rusdi, M.F.M.; Latiff, A.A.; Harun, S.W. Generation of Mode-Locked Ytterbium Doped Fiber Ring Laser Using Few-Layer Black Phosphorus as a Saturable Absorber. *IEEE J. Sel. Top. Quantum Electron.* **2017**, *23*, 39–43. [CrossRef]
19. Markom, A.M.; Tan, S.J.; Muhammad, A.R.; Paul, M.C.; Dhar, A.; Das, S.; Latiff, A.A.; Harun, S.W. Dark pulse mode-locked fibre laser with zirconia-based erbium-doped fibre (Zr-EDF) and Black phosphorus saturable absorber. *Optik* **2020**, *223*, 165635. [CrossRef]
20. Wang, C.; Peng, Q.Q.; Fan, X.W.; Liang, W.Y.; Zhang, F.; Liu, J.; Zhang, H. MXene Ti_3C_2Tx saturable absorber for pulsed laser at 1.3 mμ. *Chin. Phys. B* **2018**, *27*, 094214. [CrossRef]
21. Wang, L.; Li, X.H.; Wang, C.; Luo, W.F.; Feng, T.C.; Zhang, Y.; Zhang, H. Few-Layer Mxene Ti_3C_2Tx (T=F, O, Or OH) for Robust Pulse Generation in a Compact Er-Doped Fiber Laser. *Chemnanomat* **2019**, *5*, 1233–1238. [CrossRef]
22. Muhammad, A.R.; Jafry, A.A.A.; Markom, A.M.; Rosol, A.H.A.; Harun, S.W.; Yupapin, P. Q-Switched YDFL generation by a MAX phase saturable absorber. *Appl. Opt.* **2020**, *59*, 5408–5414. [CrossRef]
23. Jafry, A.A.A.; Kasim, N.; Rusdi, M.F.M.; Rosol, A.H.A.; Yusoff, R.A.M.; Muhammad, A.R.; Nizamani, B.; Harun, S.W. MAX phase based saturable absorber for mode-locked erbium-doped fiber laser. *Opt. Laser Technol.* **2020**, *127*, 106186. [CrossRef]
24. Shaukat, R.A.; Khan, M.U.; Saqib, Q.M.; Chougale, M.Y.; Kim, J.; Bae, J. All range highly linear and sensitive humidity sensor based on 2D material $TiSi_2$ for real-time monitoring. *Sens. Actuators B-Chem.* **2021**, *345*, 130371. [CrossRef]
25. Ma, Z.Z.; Tahersima, M.H.; Khan, S.; Sorger, V.J. Two-Dimensional Material-Based Mode Confinement Engineering in Electro-Optic Modulators. *IEEE J. Sel. Top. Quantum Electron.* **2017**, *23*, 81–88. [CrossRef]
26. Qiao, H.; Huang, Z.Y.; Ren, X.H.; Liu, S.H.; Zhang, Y.P.; Qi, X.; Zhang, H. Self-Powered Photodetectors Based on 2D Materials. *Adv. Opt. Mater.* **2020**, *8*, 1900765. [CrossRef]
27. Xie, X.; Sarkar, D.; Liu, W.; Kang, J.; Marinov, O.; Deen, M.J.; Banerjee, K. Low-frequency noise in bilayer MoS_2 transistor. *ACS Nano* **2014**, *8*, 5633–5640. [CrossRef]
28. Tiu, Z.C.; Haris, H.; Ahmad, H.; Tan, S.J. All fiber temperature sensor based on light polarization measurement utilizing graphene coated tapered fiber. *Microw. Opt. Technol. Lett.* **2021**, *63*, 1314–1318. [CrossRef]
29. Song, Y.F.; Chen, Y.X.; Jiang, X.T.; Ge, Y.Q.; Wang, Y.Z.; You, K.X.; Wang, K.; Zheng, J.L.; Ji, J.H.; Zhang, Y.P.; et al. Nonlinear Few-Layer MXene-Assisted All-Optical Wavelength Conversion at Telecommunication Band. *Adv. Opt. Mater.* **2019**, *7*, 1801777. [CrossRef]
30. Liu, W.; Shi, T.; Liu, M.; Wang, Q.; Liu, X.; Zhou, Q.; Lei, M.; Lu, P.; Yu, L.; Wei, Z. Nonlinear optical property and application of yttrium oxide in erbium-doped fiber lasers. *Opt. Express* **2021**, *29*, 29402–29411. [CrossRef]
31. Zhang, C.; Liu, J.; Gao, Y.; Li, X.; Lu, H.; Wang, Y.; Feng, J.-j.; Lu, J.; Ma, K.; Chen, X. Porous nickel oxide micron polyhedral particles for high-performance ultrafast photonics. *Opt. Laser Technol.* **2022**, *146*, 107546. [CrossRef]

32. Wang, Y.R.; Sung, W.H.; Su, X.C.; Zhao, Y.; Zhang, B.T.; Wu, C.L.; He, G.B.; Lin, Y.Y.; Liu, H.; He, J.L.; et al. Ultralow Saturation Intensity Topological Insulator Saturable Absorber for Gigahertz Mode-Locked Solid-State Lasers. *IEEE Photonics J.* **2018**, *10*, 1–10. [CrossRef]
33. Yang, J.N.; Ma, Y.J.; Tian, K.; Li, Y.H.; Dou, X.D.; Han, W.J.; Xu, H.H.; Liu, J.H. High-power passive Q-switching performance of a Yb:$YCa_4O(BO_3)_3$ laser with a few-layer Bi_2Te_3 topological insulator as a saturable absorber. *Opt. Mater. Express* **2018**, *8*, 3146–3154. [CrossRef]
34. Jafry, A.A.A.; Kasim, N.; Nizamani, B.; Muhammad, A.R.; Harun, S.W.; Yupapin, P.J.O. MAX phase Ti_3AlC_2 embedded in PVA and deposited onto D-shaped fiber as a passive Q-switcher for erbium-doped fiber laser. *Optik* **2020**, *224*, 165682. [CrossRef]
35. Chen, Y.; Zhao, C.J.; Huang, H.H.; Chen, S.Q.; Tang, P.H.; Wang, Z.T.; Lu, S.B.; Zhang, H.; Wen, S.C.; Tang, D.Y. Self-Assembled Topological Insulator: Bi_2Se_3 Membrane as a Passive Q-Switcher in an Erbium-Doped Fiber Laser. *J. Lightw. Technol.* **2013**, *31*, 2857–2863. [CrossRef]
36. Zhang, G.H.; Qin, H.J.; Teng, J.; Guo, J.D.; Guo, Q.L.; Dai, X.; Fang, Z.; Wu, K.H. Quintuple-layer epitaxy of thin films of topological insulator Bi_2Se_3. *Appl. Phys. Lett.* **2009**, *95*, 053114. [CrossRef]
37. Liu, W.; Liu, M.; Liu, X.; Wang, X.; Deng, H.-X.; Lei, M.; Wei, Z.; Wei, Z. Recent Advances of 2D Materials in Nonlinear Photonics and Fiber Lasers. *Adv. Opt. Mater.* **2020**, *8*, 1901631. [CrossRef]
38. Cheng, Z.; Li, H.; Shi, H.; Ren, J.; Yang, Q.-H.; Wang, P. Dissipative soliton resonance and reverse saturable absorption in graphene oxide mode-locked all-normal-dispersion Yb-doped fiber laser. *Opt. Express* **2015**, *23*, 7000–7006. [CrossRef]
39. Huang, S.; Wang, Y.; Peiguang, Y.; Zhang, G.; Zhao, J.; Li, H.; Lin, R.; Cao, G.; Duan, J.a. Observation of multipulse bunches in a graphene oxide passively mode-locked ytterbium-doped fiber laser with all-normal dispersion. *Appl. Phys. B* **2014**, *116*, 939–946. [CrossRef]
40. Zhao, L.M.; Tang, D.Y.; Zhang, H.; Wu, X.; Bao, Q.; Loh, K.P. Dissipative soliton operation of an ytterbium-doped fiber laser mode locked with atomic multilayer graphene. *Opt. Lett.* **2010**, *35*, 3622–3624. [CrossRef]
41. Zhao, N.; Liu, M.; Liu, H.; Zheng, X.-W.; Ning, Q.-Y.; Luo, A.-P.; Luo, Z.-C.; Xu, W.-C. Dual-wavelength rectangular pulse Yb-doped fiber laser using a microfiber-based graphene saturable absorber. *Opt. Express* **2014**, *22*, 10906–10913. [CrossRef]
42. Li, H.; Wang, Y.; Yan, P.; Cao, G.; Zhao, J.; Zhang, G.; Huang, S.; Lin, R. Passively harmonic mode locking in ytterbium-doped fiber laser with graphene oxide saturable absorber. *Opt. Eng.* **2013**, *52*, 126102. [CrossRef]
43. Chen, H.-R.; Tsai, C.-Y.; Cheng, H.-M.; Lin, K.-H.; Hsieh, W.-F. Passive mode locking of ytterbium- and erbium-doped all-fiber lasers using graphene oxide saturable absorbers. *Opt. Express* **2014**, *22*, 12880–12889. [CrossRef] [PubMed]
44. Lee, H. Monolayer MoS2-based high energy rectangular pulse fiber laser. *Optik* **2018**, *174*, 530–536. [CrossRef]
45. Cheng, P.K.; Liu, S.; Ahmed, S.; Qu, J.; Qiao, J.; Wen, Q.; Tsang, Y.H. Ultrafast Yb-Doped Fiber Laser Using Few Layers of PdS_2 Saturable Absorber. *Nanomaterials* **2020**, *10*, 2441. [CrossRef]
46. Zhang, H.; Ma, P.; Zhu, M.; Zhang, W.; Wang, G.; Fu, S. Palladium selenide as a broadband saturable absorber for ultra-fast photonics. *Nanophotonics* **2020**, *9*, 2557–2567. [CrossRef]
47. Song, H.; Wang, Q.; Zhang, Y.; Li, L. Mode-locked ytterbium-doped all-fiber lasers based on few-layer black phosphorus saturable absorbers. *Opt. Commun.* **2017**, *394*, 157–160. [CrossRef]
48. Wang, T.; Zhang, W.; Shi, X.; Wang, J.; Ding, X.; Zhang, K.; Peng, J.; Wu, J.; Zhou, P. Black phosphorus-enabled harmonic mode locking of dark pulses in a Yb-doped fiber laser. *Laser Phys. Lett.* **2019**, *16*, 085102. [CrossRef]
49. Dou, Z.; Song, Y.; Tian, J.; Liu, J.; Yu, Z.; Fang, X. Mode-locked ytterbium-doped fiber laser based on topological insulator: Bi_2Se_3. *Opt. Express* **2014**, *22*, 24055–24061. [CrossRef]
50. Chi, C.; Lee, J.; Koo, J.; Han Lee, J. All-normal-dispersion dissipative-soliton fiber laser at 1.06 μm using a bulk-structured Bi2Te3topological insulator-deposited side-polished fiber. *Laser Phys.* **2014**, *24*, 105106. [CrossRef]
51. Li, L.; Yan, P.-G.; Wang, Y.-G.; Duan, L.-N.; Sun, H.; Si, J.-H. Yb-doped passively mode-locked fiber laser with Bi_2Te_3-deposited. *Chin. Phys. B* **2015**, *24*, 124204. [CrossRef]
52. Kowalczyk, M.; Boguslawski, J.; Stachowiak, D.; Tarka, J.; Zybala, R.; Mars, K.; Mikula, A.; Sobon, G.; Sotor, J.; Abramski, K. *All-Normal Dispersion Yb-Doped Fiber Laser Mode-Locked by Sb_2Te_3 Topological Insulator*; SPIE: Bellingham, WA, USA, 2016; Volume 9893.
53. Li, L.; Wang, Y.; Wang, X.; Lin, T.; Sun, H. High energy mode-locked Yb-doped fiber laser with Bi_2Te_3 deposited on tapered-fiber. *Optik* **2017**, *142*, 470–474. [CrossRef]
54. Han, X.; Zhang, H.; Zhang, C.; Li, C.; Guo, Q.; Gao, J.; Jiang, S.; Man, B. Large-energy mode-locked ytterbium-doped linear-cavity fiber laser based on chemical vapor deposition-Bi_2Se_3 as a saturable absorber. *Appl. Opt.* **2019**, *58*, 2695–2701. [CrossRef] [PubMed]